

PHYSICAL REVIEW C

NUCLEAR PHYSICS

THIRD SERIES, VOLUME 28, NUMBER 4

OCTOBER 1983

^{11}C level structure via the $^{10}\text{B}(p,\gamma)$ reaction

M. Wiescher, R. N. Boyd, S. L. Blatt, L. J. Rybarczyk, and J. A. Spizuoco
Department of Physics, The Ohio State University, Columbus, Ohio 43210

R. E. Azuma, E. T. H. Clifford, and J. D. King
Department of Physics, University of Toronto, Toronto, Canada M5S 1A7

J. Görres, C. Rolfs, and A. Vlietks*
Institut für Kernphysik, Universität Münster, Münster, Federal Republic of Germany
(Received 12 May 1983)

The reaction $^{10}\text{B}(p,\gamma)^{11}\text{C}$ has been investigated in the energy range $E_p=0.07\text{--}2.20$ MeV. The broad resonant structure previously observed in the ground state transition near $E_p=1.2$ MeV has been seen also in γ -ray transitions to excited states. The observed excitation functions as well as the γ -ray angular distributions can be explained by assuming several broad overlapping resonances. The low-energy data ($E_p < 0.6$ MeV) reveal the existence of two s -wave resonances at $E_p=0.010$ and 0.56 MeV. Spectroscopic factors for several final states have been obtained from observation of direct capture processes to them; they are in fair agreement with results from stripping reaction studies. The present data also provide information on partial and total widths of the states at $E_x=8\text{--}9$ MeV. The energy range investigated corresponds to the temperature range of $T=(0.01\text{--}5)\times 10^9$ K. The thermonuclear reaction rates deduced from the present results are compared with previously reported values.

NUCLEAR REACTIONS $^{10}\text{B}(p,\gamma)$, $E_p=0.07\text{--}2.20$ MeV; measured γ yield for ^{11}C states up to $E_x=10.7$ MeV. Deduced resonance parameters, branching ratios, and direct capture contributions for proton-unbound states; deduced spectroscopic factors, $\Gamma_\gamma/\Gamma_{\text{tot}}$, and Γ_{tot} for several α -unbound states. Calculated thermonuclear reaction rate for $T=(0.01\text{--}5)\times 10^9$ K.

I. INTRODUCTION

The mirror nuclei ^{11}B and ^{11}C have been the subjects of many studies. As a consequence, the structure of their levels up to an excitation energy of about 8 MeV is well established. Discrepancies, some of which are indicated in Fig. 1, appear at higher excitation energies. The levels involved in these discrepancies are just unbound and could therefore be involved in the nucleosynthesis of mass 11 nuclei. For example, the rate for the $^{10}\text{B}(p,\gamma)^{11}\text{C}$ reaction might influence the production of ^{11}B , formed after β^+ decay of ^{11}C . The measured abundance ratio of $^{11}\text{B}/^{10}\text{B}$ in the interstellar medium,¹ thought to result primarily from cosmic ray spallation reactions, might depend on some stellar nucleosynthesis of this type. The reaction rate for $^{10}\text{B}(p,\gamma)^{11}\text{C}$ is only determined^{2,3} experimentally for high stellar temperatures of $T > 2 \times 10^9$ K ($T_9 > 2$), which corresponds to $E_p > 0.6$ MeV. Thus it is important to determine this reaction rate at lower temperatures (energies).

Six states have been found⁴⁻⁶ in ^{11}B at excitation energies of $E_x=9.5\text{--}11.0$ MeV, while only two states are reported for ^{11}C in the analog range of $E_x=9.0\text{--}10.5$ MeV (Fig. 1). Several experiments using different reaction channels have been carried out to investigate the level structure of ^{11}C in this energy range. The studies of the $^{10}\text{B}(p,\alpha)^7\text{Be}$ and $^{10}\text{B}(p,p)^{10}\text{B}$ reactions^{7,8} show the existence of a broad ($\Gamma \approx 250$ keV) $J^\pi = \frac{7}{2}^+$ resonance at $E_p=1.53$ MeV ($E_x=10.082$ MeV). This resonance can be identified as the analog of the $J^\pi = \frac{7}{2}^+$, $E_p=10.60$ MeV state in ^{11}B (Fig. 1). These experiments,^{7,8} as well as several $^{10}\text{B}(p,\gamma_0)^{11}\text{C}$ experiments,⁹⁻¹³ also show a strong broad resonant structure near $E_p=1.15$ MeV. However, the resonance parameters of the 1.15 MeV structures observed in the different reactions do not agree.

The excitation curves of all the $^{10}\text{B}(p,\gamma_0)^{11}\text{C}$ experiments⁹⁻¹³ indicate a resonance in this $E_p=1.15$ MeV region with a width of $\Gamma \approx 450$ keV. The angular distributions^{12,13} suggest a $J^\pi = \frac{5}{2}^-$ assignment. Recent angular distribution measurements,¹⁵ however, reveal fairly strong

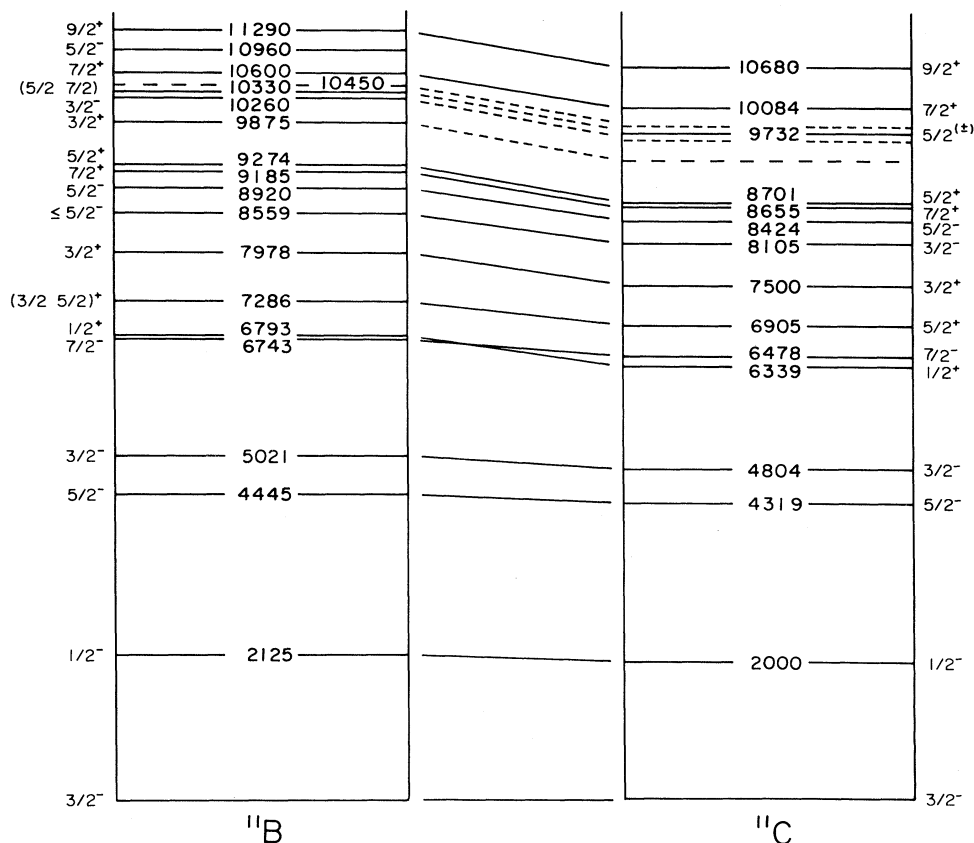


FIG. 1. Level scheme of the mirror nuclei ^{11}C and ^{11}B . The dashed lines indicate levels in ^{11}C which are expected as analogs of known levels in ^{11}B .

P_1 terms, indicating the interference of two reaction amplitudes of different parity and with a difference in orbital angular momentum of $\Delta l=1$. The $^{10}\text{B}(p,\alpha_0)^7\text{Be}$ experiments^{7,14} show a slightly sharper resonance ($\Gamma \approx 300$ keV). The isotropic α_0 angular distribution⁷ below $E_p=1.2$ MeV was interpreted to give a spin and parity assignment of $J^\pi = \frac{3}{2}^-$. The P_1 term in the measured angular distributions at $E_p=1.36$ MeV also requires the interference between two reaction amplitudes of different parity and having $\Delta l=1$. The results of the $^{10}\text{B}(p,p)^{10}\text{B}$ experiment⁸ contradict both of these J^π assignments. The scattering angular distributions below $E_p=1.2$ MeV are best fit by assuming a $J^\pi = \frac{5}{2}^+$ resonance combined coherently with a direct scattering amplitude and with contributions from the $J^\pi = \frac{7}{2}^+$ state at $E_p=1.53$ MeV. Further, at higher energies ($E_p > 1.2$ MeV), this assumption fails to fit the elastic scattering data. All these inconsistencies could be explained by the existence of several overlapping resonances.^{8,14} Detailed studies of the $^{10}\text{B}(p,\gamma)^{11}\text{C}$ reaction for a wide range of beam energies should provide sufficient information to test this hypothesis. These studies should also confirm the existence of the direct capture (DC) process in this reaction, which is expected because of the large single-particle spectroscopic factors reported from

stripping reactions. The recent measurements of Antilla *et al.*¹⁵ indicate the existence of the DC process at least to the α -unbound states at $E_x=8.424$, 8.655, and 8.701 MeV.

In view of the nuclear and astrophysical importance of the $^{10}\text{B}(p,\gamma)^{11}\text{C}$ reaction, it has been studied over the energy range of $E_p=0.07$ –2.2 MeV.

II. EXPERIMENTAL PROCEDURE

To cover the wide energy range of this experiment, studies were performed at three different accelerators. The 7 MV Super-CN Van de Graaff accelerator at Ohio State University produced a proton beam of 15–25 μA in the energy range of $E_p=0.85$ –2.2 MeV. The energy calibration of the accelerator has been determined¹⁶ to ± 1 keV, with an energy spread of 0.5 keV, using several well-known resonances.

The 1 MV Van de Graaff accelerator at the University of Toronto was used in the studies over the energy range of $E_p=0.26$ –0.96 MeV with proton beam currents of 20–70 μA . Measurements of energies of resonances in the reactions^{17–20} $^{19}\text{F}(p,\alpha\gamma)^{16}\text{O}$, $^{27}\text{Al}(p,\gamma)^{28}\text{Si}$, and $^{17}\text{O}(p,\gamma)^{18}\text{F}$ determined the energy calibration to ± 0.5 keV and the energy spread to 0.35 keV.

In the energy range of $E_p=0.07$ –0.35 MeV the 350 kV

accelerator at the University of Münster was used. This accelerator provided beam currents in the range of 150–300 μA . Energy calibration (± 0.4 keV) and beam energy spread (≤ 0.6 keV) determinations have been described elsewhere.²¹

Targets of ^{10}B with thicknesses 27, 56, and 124 $\mu\text{g}/\text{cm}^2$ were used. These targets were produced by evaporating boron (enriched to 96.19% in ^{10}B) onto a tantalum backing. The targets were able to withstand beam currents of < 200 μA without noticeable deterioration. High resolution Ge(Li) detectors (Ohio State: 70 cm^3 , Toronto: 100 cm^3 , Münster: 80 cm^3) were used to observe the reaction γ rays. The resolution of the detectors was typically 1.9–2.5 keV at $E_\gamma = 1.33$ MeV. The γ -ray efficiency for $E_\gamma = 0.5$ –12 MeV was determined by measuring (p,γ) resonances with known strengths and branching ratios^{18,22} and by using calibrated ^{60}Co and ^{56}Co sources.

The experimental setups used at the three laboratories were very similar; a typical one is shown in Fig. 2. A 1 cm diameter Ta collimator at the entrance of the chamber defined the beam spot on the target. The target itself was mounted in a water-cooled target holder situated at 45° relative to the direction of the incoming beam. A LN_2 cooled in-line copper shroud of 30 cm length in front of the target minimized carbon buildup on the target. The shroud together with the target formed the Faraday cup for beam integration. For the measurement of the excitation curves at Toronto and Ohio State the Ge(Li) detectors were positioned at 55° relative to the beam direction. In the low energy range (Münster) two Ge(Li) detectors were positioned at 0° and 90° with respect to the beam direction. At higher energies a lead plate of 1 cm thickness was placed in front of the detectors to reduce the intensity of the low-energy γ rays at 429 keV [resulting from the $^{10}\text{B}(p,\alpha\gamma)^7\text{Be}$ reaction] as well as that at 478 keV (a γ ray produced in the decay of ^7Be). The target and Ge(Li) detectors were surrounded by a 7-cm thick lead shield to reduce the room background γ rays.

With the long pulse shape necessary for optimum energy resolution with Ge(Li) detectors, pulse pileup occurs for pulse pairs arriving within any interval of less than 10 μs . With such a pileup resolving time, τ_p , the piled-up fraction of pulses, $1 - e^{-N\tau_p}$, is as large as 5% for counting rates, N , of 5000 per second. These pileup events re-

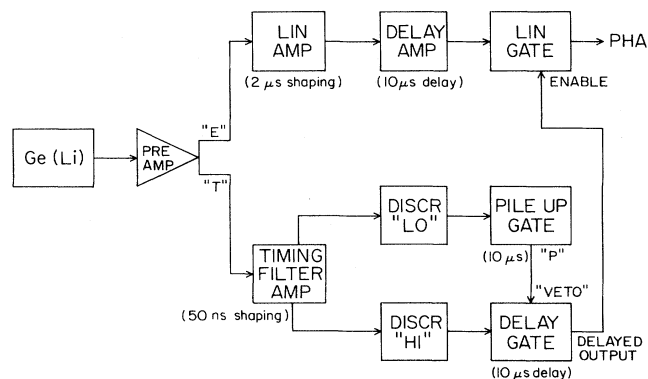


FIG. 3. Pileup circuit used to reduce pulse pileup in the γ spectra at $E_p \geq 1.2$ MeV.

sult in counts being removed from spectrum peaks, thus affecting the absolute cross section determinations. At beam energies above 1.2 MeV total counting rates of the order of 5000 pulses per second were encountered. The pileup rejection circuit (Fig. 3) examines pulses in the energy range of interest for pileup both within the preceding and succeeding 10 μs intervals, and counts the number of pulses present both before and after the rejection logic. Briefly, the system works as follows. On the timing ("T") side, short-clipped detector pulses are shaped to NIM-logic levels by a discriminator set just above the noise; these pulses are then fed into a pileup gate, which produces a pileup ("P") output if two pulses are detected with any 10 μs interval. In parallel, pulses of sufficient amplitude to be of interest for the reaction being studied are passed by a second ("HI") discriminator, and a 10 μs timing cycle is set up with a delay gate. If a pulse has preceded the pulse of potential interest within the 10 μs cycle time, the pileup gate produces a "P" output upon the arrival of the pulse of interest, which vetoes the delay gate output, thus inhibiting analysis of the piled-up pulse. If, on the other hand, the pulse of interest is followed by a second pulse within 10 μs , the "P" output is generated when the second pulse arrives; again, because of the 10 μs delay in the delay gate module, the output associated with the pulse of interest is vetoed. Finally, if the pulse of in-

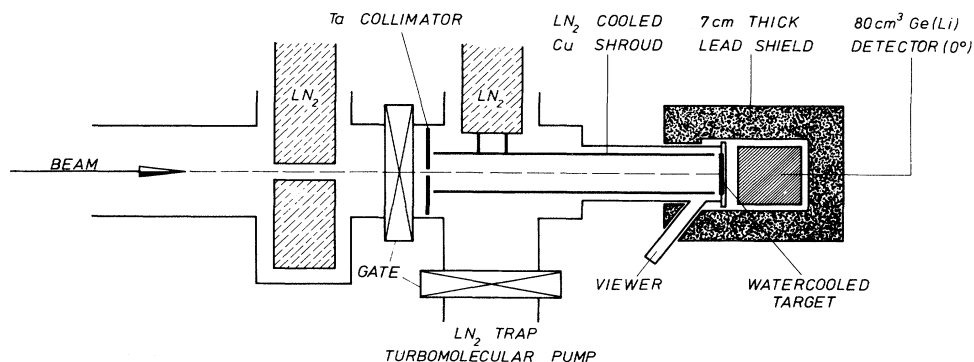


FIG. 2. Typical experimental setup used in the $^{10}\text{B}(p,\gamma)^{11}\text{C}$ studies.

terest is neither preceded nor followed, within 10 μ s, by another pulse, the output of the delay gate enables a linear gate set on the appropriately delayed linear pulse from the energy ("E") side, and it registers as part of the undistorted spectrum. Scalars on the outputs of the high discriminator and the delay gate measure the actual pileup rejection rate, from which an exact correction of the total counts in the spectrum can be made. This information allowed for corrections which reduced errors due to pileup to less than 1 percent.

In all three experimental setups, data were pulse analyzed in on-line computers and later peak fitted off line. In the study of the γ -ray angular distributions over seven angles an arrangement of two Ge(Li) detectors was used in Toronto and Ohio State. One detector was positioned at 90° relative to the beam direction and was used as a monitor. The second Ge(Li) detector, located 7 cm from the target, was rotatable over a 125° angular range. A collimator in front of the target maintained a small beam size for measuring the angular distributions. At Münster, the angular distributions over four angles were measured using a set of three Ge(Li) detectors of similar size, located 6.5 cm from the target, which were posi-

tioned at 0°, 45°, and 135°. The data at 90° were obtained from the measurement of the excitation functions at 0° and 90°.

In all of the angular distribution measurements, the relative efficiencies of the detectors were determined by observing γ -ray decays of resonances which are known to decay isotropically.

III. EXPERIMENTAL RESULTS

A. The γ -ray spectra

Figure 4 shows three γ -ray spectra, obtained at 0.126 (Münster), 0.590 (Toronto), and 1.20 MeV (Ohio State). The background lines at 6.129 MeV from the $^{19}\text{F}(p,\alpha\gamma)^{16}\text{O}$ reaction (due to ^{19}F in the tantalum backing) and at 4.44 MeV line from $^{11}\text{B}(p,\gamma)^{12}\text{C}$ (due to the small amount of ^{11}B in the target) are observable. The well-known energies of these γ -ray lines allowed the energy calibration of each spectrum to be independently determined. The primary transitions to the ground state and to the excited states at 4.319 and 6.478 MeV, as well as the secondary γ rays from these excited states, are the dominant lines in the spectra. At the higher beam energies,

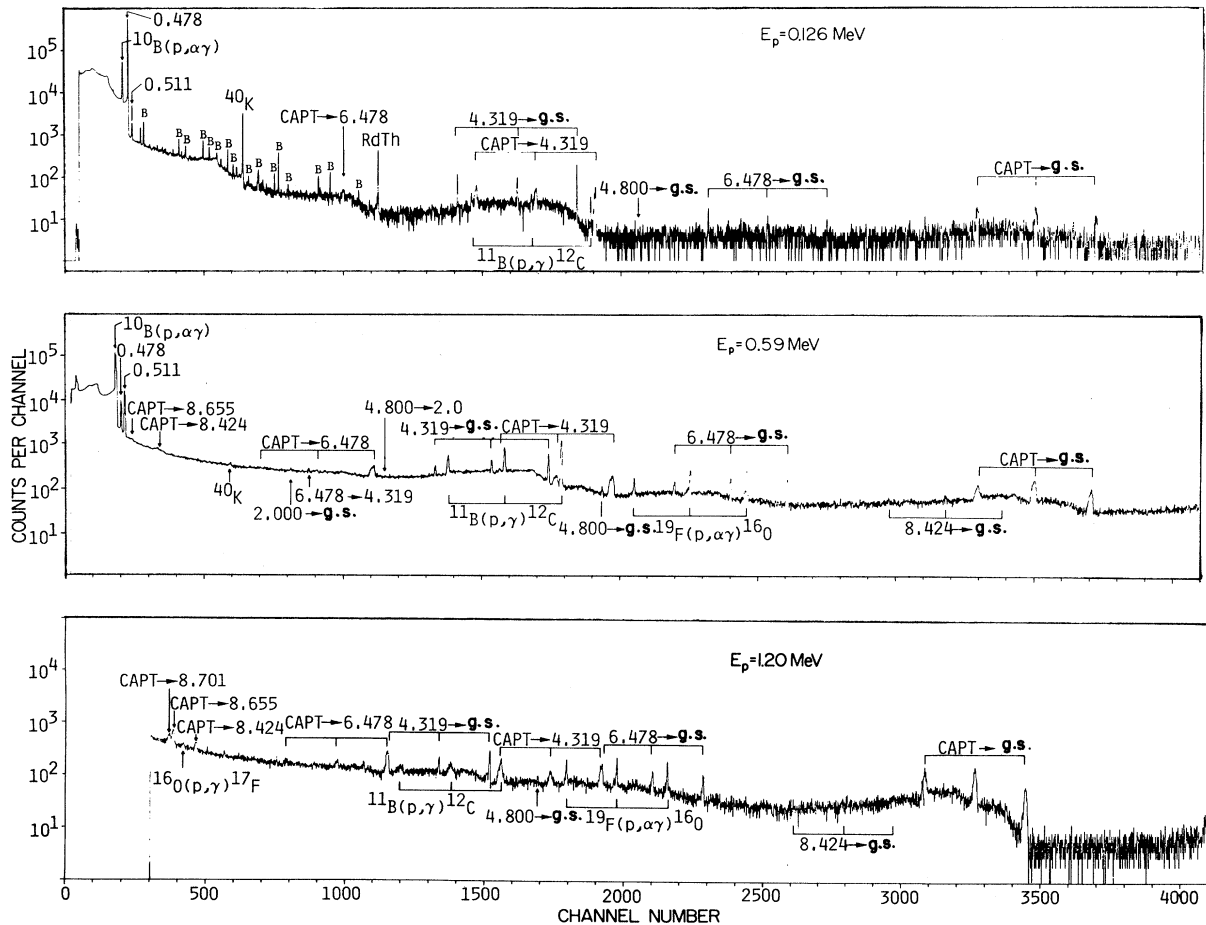


FIG. 4. Gamma ray spectra for $^{10}\text{B}(p,\gamma)^{11}\text{C}$ as obtained at the proton energies of 0.126 MeV (0°, Münster), 0.590 MeV (55°, Toronto), and 1.20 MeV (55°, Ohio State). The "B" denotes a background line.

the primary transitions to the α -unbound states at 8.424, 8.655, and 8.701 MeV are also observable.

B. Excitation functions

The excitation curves for all observed primary and secondary γ -ray transitions were determined. Figure 5 shows the excitation curves for the dominant transitions. The absolute cross sections were determined relative to the strengths $\omega\gamma$ of known resonances using the relation

$$\sigma = \frac{\lambda^2 \pi^2}{2\Delta} \frac{m_T + m_p}{m_T} \frac{Y(E)}{Y_{\text{res}}} \omega\gamma. \quad (1)$$

In this equation, $Y(E)$ is the $^{10}\text{B}(p,\gamma)$ γ -ray yield, Y_{res} is the thick target yield of the reference resonance, λ is the wavelength in the c.m. system, Δ is the ^{10}B target thickness, and m_T (m_p) is the ^{10}B (proton) mass. The resonance energies and resonance parameters used are listed in Table I. The cross section normalizations, involving target thickness, beam integration, and detector efficiency,

were carried out independently for each experimental set-up. In the overlapping energy regions of the different accelerators used, the resulting cross sections agreed with each other. The indicated uncertainties include statistical effects (5–20%), uncertainties in the resonance strengths of the reference resonances (see Table I), and uncertainties in the efficiency determination (5%) and in the determination of the target thickness (5%).

Previous work^{9–13} determined only the excitation curve for the ground state transition in the energy range of $E_p = 0.6$ –2.2 MeV. The energy dependence of that excitation curve as well as the value of the absolute cross section obtained in the present work agrees well with previous data. The structures observed in the excitation curves are discussed in Sec. IV A.

C. Angular distributions

The γ -ray angular distributions were measured at several beam energies: $E_p = 0.125, 0.226, 0.325, 0.360, 0.500, 0.700, 0.850, 1.150, 1.250,$ and 1.550 MeV. For the

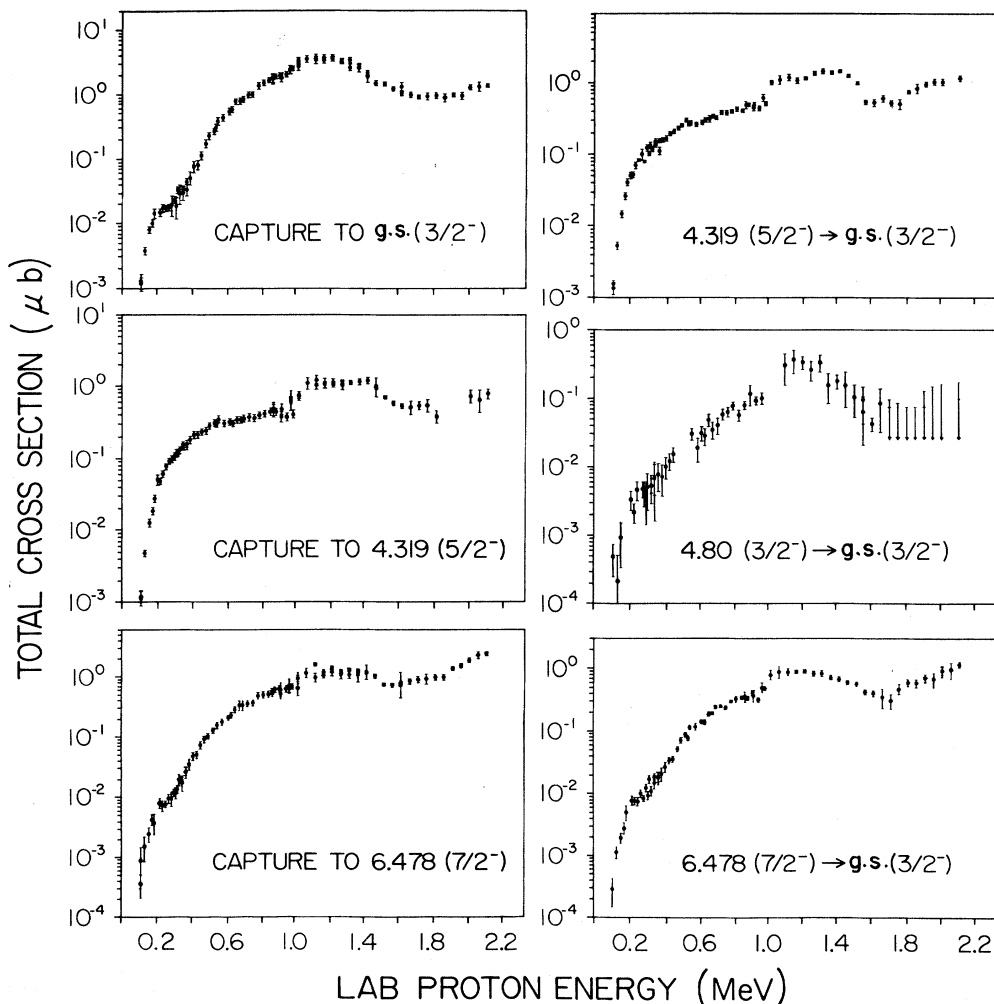


FIG. 5. Excitation curves for observed primary γ transitions to the ground state and the states at 4.319 and 6.478 MeV. Also shown are the curves for the secondary decays to the ground state. The total cross sections shown are not corrected for forward-backward asymmetries [that is, $\sigma = 4\pi \times d\sigma/d\Omega(55^\circ)$].

TABLE I. Reference resonances used for the energy calibration of the accelerator and for determination of the cross section of $^{10}\text{B}(p,\gamma)^{11}\text{C}$.

Location	Reaction	Resonance energy (MeV)	Strength $\omega\gamma$ (eV)	Refs.
Münster	$^{14}\text{N}(p,\gamma)^{15}\text{O}$	0.278	$1.4 \pm 0.1 \times 10^{-2}$	18
	$^{27}\text{Al}(p,\gamma)^{28}\text{Si}$	0.327	$1.9 \pm 0.41 \times 10^{-3}$	19
Toronto	$^{27}\text{Al}(p,\gamma)^{28}\text{Si}$	0.327	$1.9 \pm 0.41 \times 10^{-3}$	19
	$^{27}\text{Al}(p,\gamma)^{28}\text{Si}$	0.991	1.93 ± 0.13	17,19,22
	$^{17}\text{O}(p,\gamma)^{18}\text{F}$	0.582	0.32 ± 0.09^a	20
Ohio State	$^{27}\text{Al}(p,\gamma)^{28}\text{Si}$	0.991	1.93 ± 0.13	17,19,22

^aResonance strength calculated relative to that of the 0.991 MeV resonance in $^{27}\text{Al}(p,\gamma)^{28}\text{Si}$.

first three energies, the measurements were performed at the angles of 0° , 45° , 90° , and 135° and for the latter energies at the angles of 0° , 30° , 45° , 60° , 90° , and 120° . Owing to the generally small cross sections, the angular distributions were obtained only for the strongest transitions. The data are well represented by a_1 and a_2 terms resulting from Legendre polynomial fits to the angular distributions²³ (and are shown in Fig. 7). The indicated uncertainties are the standard deviations in χ^2 resulting from the fits to the angular distribution data, and thus include implicitly all the data uncertainties discussed above, as well as the geometrical and normalization uncertainties associated with measurement of the angular distributions. While the angular distributions for the transitions to the ground state, the 4.319 MeV state, and the 6.478 MeV state are essentially isotropic at energies below $E_p = 0.8$ MeV, strong anisotropies show up above $E_p = 0.9$ MeV (Fig. 7). This observation is in good agreement with previous results.^{12,13,15}

IV. DISCUSSION

A. Resonance structures

It has previously been assumed (Sec. I) that one 0.5-MeV wide resonance near $E_p = 1.15$ MeV dominates the strength of the ground state transition. This explanation, however, causes difficulties in the comparison of the results obtained for the different reactions^{7,8,13} and results in inconsistencies in J^π assignments and widths. It has been suggested^{8,14} that these difficulties could be removed if additional resonance structures exist in ^{11}C with different spins and parities. The ^{11}B level scheme suggests that at least three more states can be expected in ^{11}C at excitation energies of $E_x = 9-10$ MeV. We therefore tried to understand, and to fit, our data in terms of this picture.

Figure 6 shows the S -factor² curves for the three strongest primary γ -ray transitions. Those curves for all transitions were fit assuming the existence of four to seven resonances based either on established states in ^{11}C or on those suggested by analogy to ^{11}B . A direct capture (DC) contribution was also assumed for transitions to states having fairly large single-particle spectroscopic factors²⁴ (C^2S). The function used to fit the data is

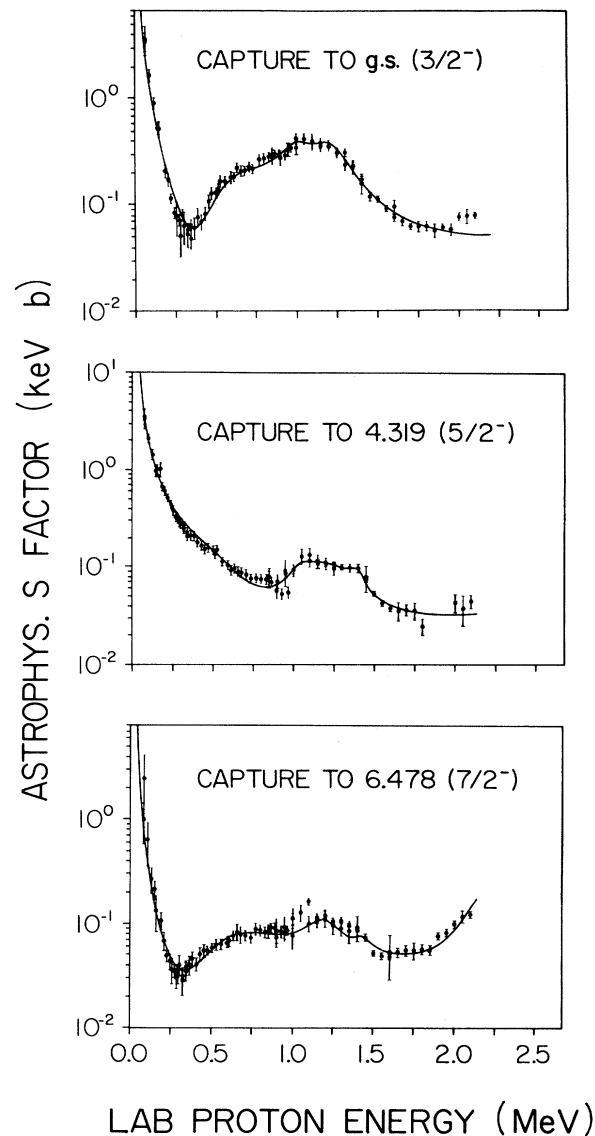


FIG. 6. Optimal fits through the S factor data of the ground state transition and of the transitions to the states of 4.319 and 6.478 MeV. The fit parameters are listed in Table II.

$$S(E, 55^\circ) = \sum_{i=1}^N S_{Ri}(E) + S_{\text{DC}}(E) + 2 \sum_i \sum_k [S_{Ri}(E)S_{\text{DC}}(E)]^{1/2} W_{i\text{DC}}(k) \cos \delta_i P_k(55^\circ) \\ + 2 \sum_i \sum_{\substack{j \\ i < j}} \sum_k [S_{Ri}(E)S_{Rj}(E)]^{1/2} W_{ij}(k) \cos \delta_{ij} P_k(55^\circ). \quad (2)$$

The S -factor curve $S_{Ri}(E)$ for each of the resonances was described by a Breit-Wigner shape where corrections for the energy dependence of the partial widths have been taken into account. The DC contribution was described by a polynomial function

$$S_{\text{DC}}(E) = C^2 S(S_0 + S'E + \frac{1}{2}S''E^2),$$

where the parameters S_0 , S' , and S'' resulted from the DC model calculations.²⁵ The last two terms in Eq. (2) describes possible interference effects between the DC process and the single resonances as well as interference effects between the resonances themselves. The resonance phases, the Coulomb phases, and the hard sphere phases are included in the phases δ_i and δ_{ij} , while the interference term $W_{i\text{DC}}(k)$ is given in Eq. (A38) of Ref. 25, and $W_{ij}(k)$ is included in Eq. (6.22) of Ref. 26.

Since the excitation functions shown in Fig. 5 give the cross section at 55° (at which $P_2=0$), only angular distribution and interference effects for $k \leq 1$ terms need to be considered in the fitting procedures for them. The free parameters used in the data fitting were resonance energy, width, and amplitude. For the additional new states in ^{11}C various J^π assignments were examined using the possible values of the analog states in ^{11}B as a guide. The final resonance parameters were determined after several iterations involving all three transitions. The resulting fits are shown in Fig. 6.

1. Ground state transition

The excitation function of the transition to the $J^\pi = \frac{3}{2}^-$ ground state can be fitted by assuming four resonances centered at $E_p = 0.01, 0.56, 1.05,$ and 1.20 MeV, and a DC contribution. While the strong s -wave resonance at $E_p = 0.01$ MeV corresponds to the known $J^\pi = \frac{5}{2}^+$ state at $E_x = 8.701$ MeV, the second resonance, at $E_p = 0.56$ MeV, has not been previously identified. The possible analog state in ^{11}B (Fig. 1) was thought to be the $J^\pi = \frac{3}{2}^+$ state^{4-6,27} at $E_x = 9.88$ MeV. However, it was not possible to fit the present data in the energy range of $E_p = 0.2-0.5$ MeV assuming a $\frac{3}{2}^+$ resonance. Only strong, destructive, angle-independent interference between the $E_p = 0.01$ and 0.56 MeV resonances can explain the low energy structure of this S -factor curve; this could be achieved only with a $J^\pi = \frac{3}{2}^+$ assignment for the $E_p = 0.56$ MeV resonance. This assignment is supported also by the S -factor curves of the two other transitions (Fig. 6), which are also explainable by assuming two interfering s -wave resonances plus a DC amplitude. Figure 7 shows the energy dependence of the a_1 and a_2 terms, calculated from the resonance parameters, in comparison

with the measured angular distribution data. For all three transitions the measured isotropy below $E_p = 0.8$ MeV is in reasonable agreement with the angular distribution predicted with this resonance structure.

The present results for the ground state transition suggest also the existence of at least two overlapping resonances contributing to the yield of the broad structure above 1 MeV (Fig. 6). Such a description resolves discrepancies discussed above in which a single broad resonance was assumed. The explanation of the structure by $J^\pi = \frac{3}{2}^-$ and $J^\pi = \frac{5}{2}^-$ resonances as well as s - and d -wave DC contributions provides a good representation. This assumed description is also consistent with the structure of the analog nucleus (Fig. 1). The interference between the negative parity resonances and the combination of the DC process and the strong low energy s -wave resonances produces a_1 terms in the angular distributions; these are observed in the present work (Fig. 7) as well as in previous work.¹⁵ The observed energy dependence of the a_2 terms is also explainable in this picture (Fig. 7).

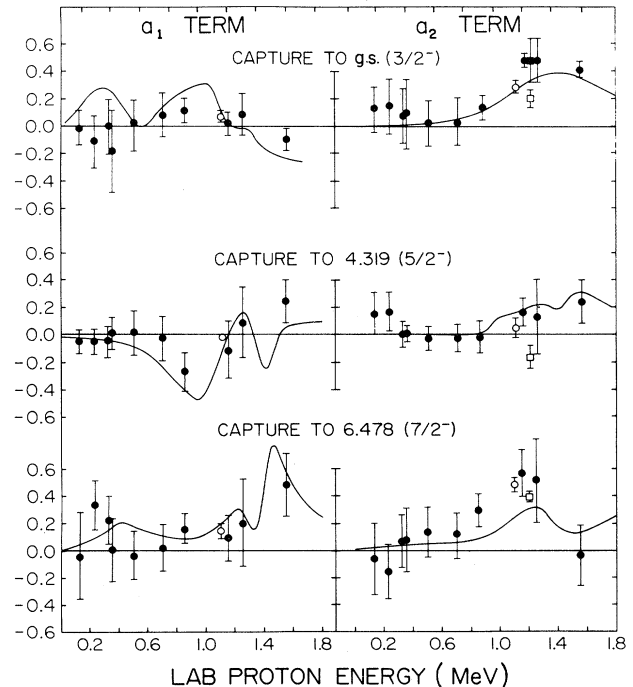


FIG. 7. Experimental a_1 and a_2 terms (present results are indicated as the solid circles) resulting from a Legendre polynomial fit to the measured angular distributions. The open circles are results of Ref. 15, open squares of Ref. 13, and solid squares of Ref. 12. The solid curves describe the calculated energy dependence of the a_1 and a_2 terms based on the fits shown in Fig. 6 and Table II.

TABLE II. Resonance parameters resulting from the fit procedure described in Sec. IV A.

E_R (MeV)	E_x (MeV)	J^π	Γ_{tot} (MeV)	σ_{res} (μb)	Ref.
0.010±0.002	8.701±0.01	$\frac{5}{2}^+$	0.016±0.001	$(2.07\pm0.40)\times 10^{-14}^a$	
0.56 ±0.06	9.20 ±0.05	$\frac{5}{2}^+$	0.55 ±0.10	0.28 ±0.05	
1.05 ±0.06	9.65 ±0.05	$(\frac{3}{2}^-)$	0.23 ±0.05	2.06 ±0.60	
1.20 ±0.05	9.79 ±0.05	$(\frac{5}{2}^-)$	0.26 ±0.06	3.69 ±0.72	
1.41 ±0.05	9.97 ±0.05	$(\frac{7}{2}^-)$	0.13 ±0.02	0.75 ±0.20	
1.53	10.082	$\frac{7}{2}^+$	0.23	0.022±0.015	7,8
2.19	10.682	$\frac{9}{2}^+$	0.28	2.66 ±0.85	8

^aResulting from the extrapolation to lower energies.

2. Transitions to the $\frac{5}{2}^-$ (4.319 MeV) and $\frac{7}{2}^-$ (6.478 MeV) levels

For the transition to the $J^\pi = \frac{5}{2}^-$ state at $E_x = 4.319$ MeV (Fig. 6), an additional $J^\pi = \frac{7}{2}^-$ resonance at $E_p = 1.41$ MeV as well as a $J^\pi = \frac{7}{2}^+$ resonance at $E_p = 1.53$ MeV had to be included in order to fit the data. The latter resonance was already observed in previous studies^{7,8} of the $^{10}\text{B}(p,\alpha)^7\text{Be}$ and $^{10}\text{B}(p,p)^{10}\text{B}$ reactions. The $J^\pi = \frac{7}{2}^-$ state might be the analog state of that at $E_x = 10.33$ MeV in ^{11}B , which has previously been assigned⁶ a J^π of $\frac{5}{2}^+$, although that assignment did not give a good fit to the data in Ref. 6. The present spin and par-

ity assignment, $J^\pi = \frac{7}{2}^-$, is supported by the existence of strong a_1 terms in the angular distributions at $E_p = 1.55$ MeV, which would naturally result from the interference between these $J^\pi = \frac{7}{2}^-$ and $\frac{7}{2}^+$ resonances.

The excitation curve of the transition to the $J^\pi = \frac{7}{2}^-$ state at $E_x = 6.478$ MeV between $E_p = 0.8$ –1.8 MeV (Fig. 6) is explainable by the influence of the $J^\pi = \frac{5}{2}^-$ resonance at 1.20 MeV, the $J^\pi = \frac{7}{2}^-$ resonance at 1.41 MeV, and the $J^\pi = \frac{7}{2}^+$ resonance at 1.53 MeV, as well as the DC contributions. Again the interference between the two $J = \frac{7}{2}$ resonances produces the strong a_1 term at $E_p = 1.55$ MeV. Representation of the shape of the S -factor curve above $E_p = 1.7$ MeV requires the $J^\pi = \frac{9}{2}^+$ resonance at 2.15 MeV, which has been measured in the $^{10}\text{B}(p,p)^{10}\text{B}$ reaction.⁸ Table II shows the parameters of all the proposed states resulting from the fitting procedures. The branching ratios for these proposed resonances are given in Table III.

Although the data above 1 MeV are well represented by the J^π assignments discussed above, the uniqueness of those assignments is difficult to establish. However, within the wide variety of J^π assignments which were tried for the levels for which J^π is uncertain, only the values stated above provided good fits to all the available data. Measurements in other reaction channels or analyzing power data might be useful, in conjunction with the present results, in providing unambiguous J^π assignments.

B. Structure of the α -unbound and the p -unbound states in ^{11}C

Four states are known in the excitation energy range between 8 and 9 MeV. The capture to the states at 8.424 MeV ($\frac{5}{2}^-$), 8.655 MeV ($\frac{7}{2}^+$), and 8.701 MeV ($\frac{5}{2}^+$) could be observed in the energy range of $E_p = 0.5$ –2.2 MeV, while only an upper limit for the proton capture to the state at 8.105 MeV ($\frac{3}{2}^-$) could be determined. Figure 8 shows the excitation curves for these transitions. The cross sections and uncertainties were obtained as indicated in Sec. III B. The excitation curves can be described in terms of the DC model²⁵ (Fig. 8). For the transition to the state at 8.424 MeV weak interference effects seem to influence the excitation curve in the range $E_p = 0.6$ –1.3

TABLE III. Branching for the proposed states resulting from the fitting procedures.

E_i (MeV)	J_i^π	E_f (MeV)	J_f^π	Branching (%)
8.701	$\frac{5}{2}^+$	0	$\frac{3}{2}^-$	42±10
		4.319	$\frac{5}{2}^-$	42±10
		4.802	$\frac{3}{2}^-$	2.4± 1.5
		6.478	$\frac{7}{2}^-$	13.6± 4.6
9.200	$\frac{5}{2}^+$	0	$\frac{3}{2}^-$	74±18
		4.319	$\frac{5}{2}^-$	6± 5
		6.478	$\frac{7}{2}^-$	20±10
9.650	$(\frac{3}{2}^-)$	0	$\frac{3}{2}^-$	60±15
		4.319	$\frac{5}{2}^-$	32±10
		4.802	$\frac{3}{2}^-$	8± 4
9.79	$(\frac{5}{2}^-)$	0	$\frac{3}{2}^-$	76±16
		4.319	$\frac{5}{2}^-$	8± 2
		4.802	$\frac{3}{2}^-$	4± 2
		6.478	$\frac{7}{2}^-$	12± 4
9.97	$(\frac{7}{2}^-)$	4.319	$\frac{5}{2}^-$	90±10
		6.478	$\frac{7}{2}^-$	10± 7
10.082	$\frac{7}{2}^+$	4.319	$\frac{5}{2}^-$	67± 8
		6.478	$\frac{7}{2}^-$	13± 6
10.682	$\frac{9}{2}^+$	6.478	$\frac{7}{2}^-$	100

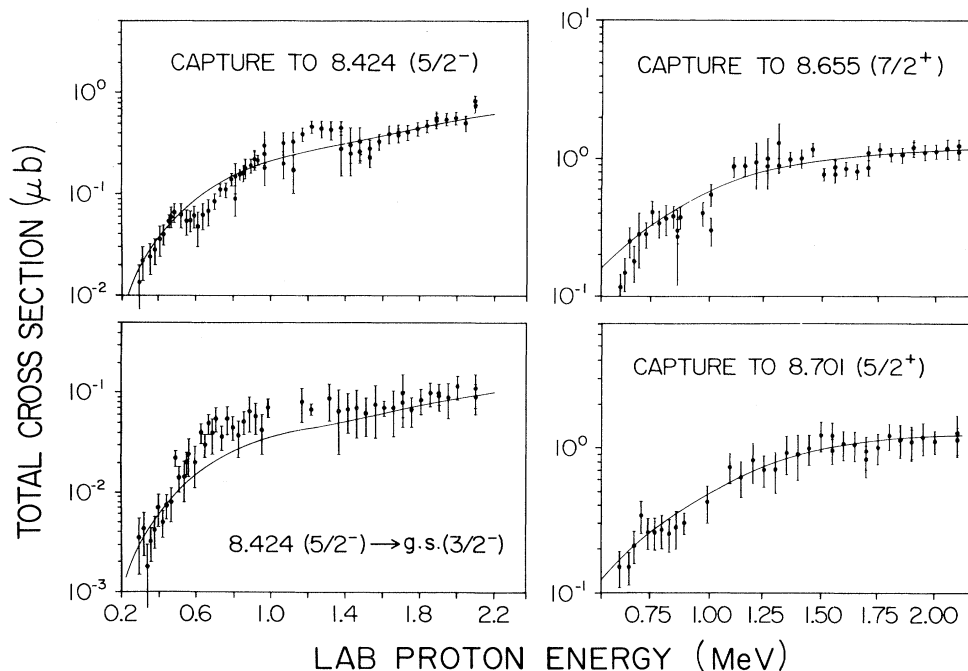


FIG. 8. Excitation functions for the capture transitions to the α -unbound states in ^{11}C at $E_x = 8.424$, 8.655 , and 8.701 MeV, and for the observed decay transition 8.424 MeV \rightarrow g.s. The total cross section shown is not corrected for forward-backward asymmetry [that is, $\sigma = 4\pi \times d\sigma/d\Omega(55^\circ)$]. The solid line shows the result of a direct capture calculation scaled to the data. The scaling factors are equivalent to the spectroscopic factors of the final states and are listed in Table V.

MeV. This might be the result of the broad resonance described in the last section. But the DC contribution clearly dominates the yield of the excitation curve.

The angular distributions for all of these transitions were measured at $E_0 = 1.15$ and 1.55 MeV, and were fit²³ by Legendre polynomials. The resulting a_2 terms are compared with those calculated in terms of the DC model.²⁵ The results are listed in Table IV. The excellent agreement supports the assumption of the DC character of these transitions. The slight forward-backward asymmetry, suggesting the need of an a_1 term in fitting the angular distributions of the transition¹⁵ to the state at 8.424 MeV, might be due to the influence of the weak interference effect discussed above.

The spectroscopic factors of these states $C^2S = \sigma(\text{exp})/\sigma(\text{theo})$ result from the fitting of the theoretical curves to the data. The results are compared in Table V with the corresponding values from stripping reactions.²⁸⁻³⁰

The fairly strong population of these states by the (p,γ) reaction allows the possibility of observing the secondary γ -ray decays from them, even though they would be expected to decay predominantly into the α channel. The ratio of the γ -ray yield of such a secondary transition yield to the primary one determines the ratio $\Gamma_\gamma/\Gamma_{\text{tot}}$. In the present measurements, secondary transitions could be observed in the ground-state decay of the state at 8.424 MeV. The excitation curve for that transition is shown in Fig. 8. As in the primary transition, a suggestion of weak resonant contributions is also observed here. Only upper limits could be determined for the possible decay transitions of the states at 8.655 and 8.701 MeV. The results are listed in Table VI, where they are compared with the results of previous work.

The state at $E_x = 8.701$ MeV is slightly proton unbound, and is observed both as a final state in primary capture transitions, and as a strong resonance at $E_p = 0.01$ MeV (Sec. IV B). The high energy tail of this resonance had

TABLE IV. Angular distribution parameters for transitions to the α -unbound states $E_x < 9$ MeV.

E_x (final) (MeV)	l_i	l_f	$E_p = 1.11$ MeV ^a		a_2 coefficient $E_p = 1.15$ MeV		$E_p = 1.55$ MeV	
			Theo	Exp	Theo	Exp	Theo	Exp
8.424	s, d^b	p	0.53	0.45 ± 0.04	0.53	0.46 ± 0.18	0.70	0.52 ± 0.27
8.655	p	s, d^c	-0.92	-1.06 ± 0.07	-0.92	-0.89 ± 0.17	-0.75	-0.71 ± 0.08
8.701	p	s, d^c	-0.92	-1.2 ± 0.06	-0.92	-0.94 ± 0.15	-0.75	-0.75 ± 0.09

^aReference 15.

^bUsing Eq. (12), Ref. 25.

^cUsing Eq. (12), Ref. 25. The d - to s -wave ratio σ_d/σ_s resulted from the theoretical direct capture calculations.

TABLE V. Spectroscopic factors C^2S for the α -unbound states in ^{11}C .

E_x (MeV)	J_f^π	Direct capture C^2S	Stripping data C^2S^a	$^{10}\text{B}(^3\text{He,d})$ C^2S^b	C^2S^c
8.105	$\frac{3}{2}^-$	<0.05		0.07	
8.424	$\frac{5}{2}^-$	0.39 ± 0.04	0.46	0.73, 0.79	
8.655	$\frac{7}{2}^+$	0.26 ± 0.03	0.33	0.41	0.18
8.701	$\frac{5}{2}^+$	0.31 ± 0.03	0.14	<0.8	0.2

^aReference 28.^bReference 29.^cReference 30.

been observed, but misinterpreted, in an earlier $^{10}\text{B}(p,\alpha)^7\text{Be}$ experiment.³¹ It was observed again in a recent unpublished $^{10}\text{B}(p,\alpha)$ experiment.³² The ratio $\Gamma_\gamma/\Gamma_{\text{tot}}$ could be calculated from the ratio of the cross sections in the γ -ray and α -particle channels, $\sigma(p,\gamma)/\sigma(p,\alpha)$. This result is also listed in Table VI.

The widths of the γ -ray peaks in the spectra for these particular transitions were determined for several targets with different target thicknesses Δ . This allows, after correction for the experimental resolution, calculation of the total width Γ_{tot} of the final state if $\Gamma_{\text{tot}} > \Delta$, or at least the upper limit of the total width when $\Gamma_{\text{tot}} < \Delta$. The tar-

get thickness Δ was assumed to be equivalent to the γ -ray peak width of the transitions to the ground state and the states at $E_x = 4.319$ MeV and $E_x = 6.478$ MeV, whose widths are negligible compared with the target thickness. The widths obtained for the 8.424, 8.655, and 8.701 MeV states are also presented in Table VI.

V. Astrophysical implications

The reaction rate $N_A \langle \sigma v \rangle$ was obtained by numerical integration of the total $S(E)$ curve over the Maxwell-Boltzmann distribution using the expression²

$$N_A \langle \sigma v \rangle = \left[\frac{8}{\pi \mu} \right]^{1/2} \frac{N_A}{(kT)^{3/2}} \int_0^{E_{\text{max}}} S(E) \exp \left[-\frac{E}{kT} - 2\pi\eta \right] dE, \quad (3)$$

where μ is the reduced mass, k the Boltzmann constant, η the Sommerfeld parameter, E the particle energy in the center of mass system, and T the temperature.

The total S factor is defined as the sum of the S factors of all primary transitions involved: $S(E) = \sum_i S_i(E)$. In the energy range below $E_p = 0.07$ MeV, no experimental data are available. In this case S factors resulting from the described fitting procedures were used to calculate the reaction rates.

The upper limit E_{max} for the integration was given by the highest energy investigated ($E_p = 2.2$ MeV). This energy limits the validity of the resulting reaction rates to a temperature range of $T_9 = 0.01$ to 5. The resulting rates were fitted by analytic expressions and are described by

$$N_A \langle \sigma v \rangle = T_9^{-3/2} \exp(16.665 - 13.2145T_9^{-1/3} + 0.6854T_9^{-2/3} - 9.0545E - 2T_9^{-1}) \\ \times (1 - 0.83145T_9^{1/3} - 0.10218T_9^{2/3} + 0.03238T_9 + 0.3936T_9^{4/3} - 0.005790T_9^{5/3}). \quad (4)$$

TABLE VI. Widths of low-lying α -unbound states in ^{11}C .

E_x (MeV)	$\Gamma_\gamma/\Gamma_{\text{tot}}$		Γ_{tot}	
	Present	Previous	Present	Previous
8.424	0.20 ± 0.05	0.2 ± 0.1^c 0.8 ± 0.2^d	≤ 5 keV	< 23 fs ^d
8.655	< 0.06		≤ 5 keV	≤ 9 keV ^c
8.701	$(2.6 \pm 0.15) \times 10^{-4a}$ $\leq 0.1^b$		16 ± 1 keV ^a 14.5 ± 2.5 keV ^b	15 ± 1 keV ^c

^aBased on resonance parameters.^bBased on direct capture data.^cReference 36.^dReference 15.

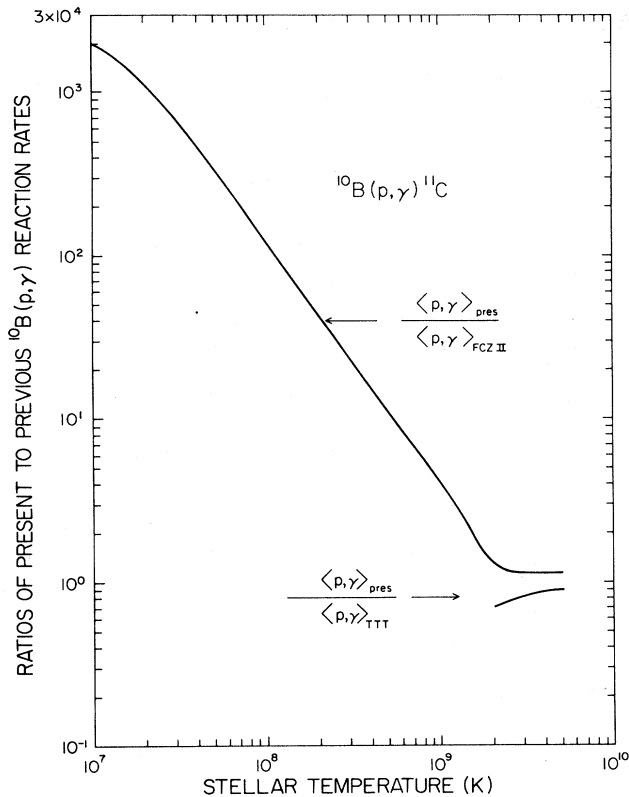


FIG. 9. Ratios of the reaction rates of $^{10}\text{B}(p,\gamma)^{11}\text{C}$ in the present work to those of previous work [FCZII (Ref. 2), TTT (Refs. 3 and 33)] as a function of temperature.

The deviations of the numerically integrated rates from those obtained by the analytic expression are on the average smaller than 5%. Figure 9 compares the present results with the estimates of Fowler, Caughlin, and Zimmerman² (FCZII), which were based on previously available data at $E_p \geq 0.6$ MeV. The disagreement in the low temperature region is due predominantly to the observed strong s -wave resonance at $E_R = 0.01$ MeV and the interference effects with the second s -wave resonance at $E_R = 0.56$ MeV. The present results and the reaction rates based on a $^{10}\text{B}(p,\gamma)^{11}\text{C}$ measurement³ using a thick-target technique³³ (TTT) are in fair agreement (Fig. 9). Figure 10 shows the comparison between the present (p,γ) reaction rate and rates reported for the competing reaction $^{10}\text{B}(p,\alpha)^7\text{Be}$. The rate published in FCZII does not include the low energy resonance at $E_R = 0.01$ MeV, which is expected to decay predominantly by α -particle emission (Table VI). The reaction rate for $^{10}\text{B}(p,\alpha)^7\text{Be}$ has therefore been recalculated using Eq. (3) and data from other experiments^{31,34,35} covering the energy range of $E_p = 0.06$ –2.0 MeV (denoted as “calc” in Fig. 10). The low energy data could be fit by the high energy tail of the $E_R = 0.01$ MeV resonance, which dominates the reaction rate at low temperatures. The comparison of the $^{10}\text{B}(p,\gamma)^{11}\text{C}$ rates and the calculated $^{10}\text{B}(p,\alpha)^7\text{Be}$ rates is also presented in Fig. 10.

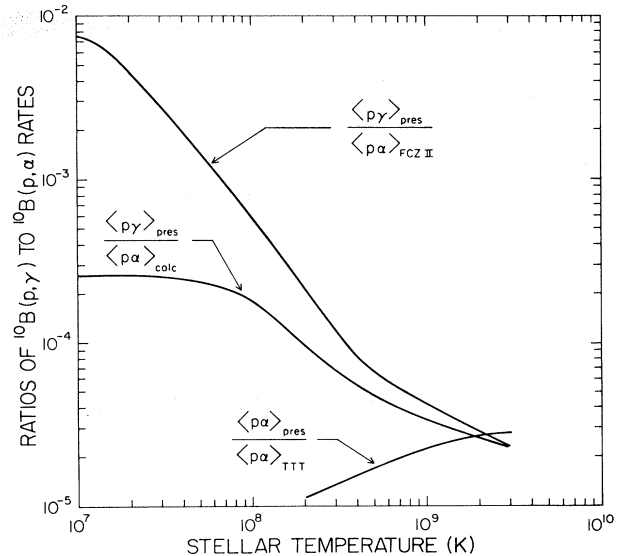


FIG. 10. Ratio of the reaction rate for $^{10}\text{B}(p,\gamma)^{11}\text{C}$ to rates given for the competitive reaction $^{10}\text{B}(p,\alpha)^7\text{Be}$ [FCZII (Ref. 2), TTT (Refs. 3 and 33), and calc (see the discussion in Sec. V)] as a function of temperature.

The third curve in the figure shows the ratio of the $^{10}\text{B}(p,\gamma)^{11}\text{C}$ rate to a $^{10}\text{B}(p,\alpha)^7\text{Be}$ rate³ determined by the thick-target technique³³ (TTT). The latter reaction rate also includes the influence of the resonance at $E_R = 0.01$ MeV. This curve varies considerably at low temperatures from those based on thin-target experiments but at high temperatures the three ratios agree fairly well with each other (Fig. 10). According to the result of the thick-target experiment, the resonance strength of the $E_R = 0.01$ MeV resonance would be about a factor of 10 larger than that determined from the thin-target experiments.^{31,35} The use of the thick target result would give a significantly smaller value for the γ partial width of this particular state, $\Gamma_\gamma \approx 0.2$ eV. This is in disagreement with the known γ partial width of the ^{11}B analog state at $E_x = 9.59$ MeV, $\Gamma_\gamma = 2.3$ eV,²⁴ which is comparable to the γ width of the ^{11}C state determined from the results of other thin-target experiments (Table VI), namely, 4.2 eV. A careful investigation of the $^{10}\text{B}(p,\alpha)^7\text{Be}$ reaction below $E_p = 1$ MeV is needed to clarify the situation.

ACKNOWLEDGMENTS

The authors wish to thank B. Sur, Y. Lee, R. Turner, and P. Schmalbrock for their assistance in the data taking, and M. J. Gallant for making some of the ^{10}B targets. This work was supported by the U.S. National Science Foundation, the Natural Sciences and Engineering Research Council of Canada, and the Deutsche Forschungsgemeinschaft.

- *Present address: Litton Industries, 960 Industrial Rd., San Carlos, CA 94070.
- ¹S. Austin, *Prog. Part. Nucl. Phys.* **7**, 1 (1981).
- ²W. A. Fowler, G. R. Caughlin, and B. A. Zimmerman, *Ann. Rev. Astron. Astrophys.* **13**, 69 (1975).
- ³R. J. Peterson, C. S. Zaidin, M. J. Fritts, N. A. Roughton, and C. J. Hansen, *Ann. Nucl. Energy* **2**, 503 (1975).
- ⁴R. Y. Cusson, *Nucl. Phys.* **86**, 481 (1966).
- ⁵P. Paul, N. G. Puttaswamy, and D. Kohler, *Phys. Rev.* **164**, 1332 (1967).
- ⁶J. P. Stoquert, N. Bendjaballah, H. Beaumevielle, G. Gerardin, and R. Seltz, *J. Phys. (Paris)* **40**, 813 (1979).
- ⁷J. W. Cronin, *Phys. Rev.* **101**, 298 (1956).
- ⁸J. C. Overley and W. Whaling, *Phys. Rev.* **128**, 315 (1962).
- ⁹R. W. Krone and L. W. Seagondollar, *Phys. Rev.* **92**, 935 (1953).
- ¹⁰R. B. Day and T. Huus, *Phys. Rev.* **95**, 1003 (1954).
- ¹¹S. E. Hunt, R. A. Pope, and W. W. Evans, *Phys. Rev.* **106**, 1012 (1957).
- ¹²G. B. Chadwick, T. K. Alexander, and J. B. Warren, *Can. J. Phys.* **34**, 381 (1956).
- ¹³A. N. James, *Nucl. Phys.* **24**, 675 (1961).
- ¹⁴A. B. Brown, C. W. Snyder, W. A. Fowler, and C. C. Lauritsen, *Phys. Rev.* **82**, 159 (1951).
- ¹⁵A. Antilla, J. Keinonen, and R. Hentelä, *Phys. Rev. C* **20**, 920 (1979).
- ¹⁶T. C. Rinckel, A. K. Basak, T. R. Donoghue, C. Rolfs, and K. E. Sale, Ohio State University Van de Graaff Laboratory report, 1982 (unpublished), p. 130.
- ¹⁷A. Antilla, J. Keinonen, M. Hautala, and I. Forsblom, *Nucl. Instrum. Methods* **147**, 501 (1977).
- ¹⁸H. W. Becker, W. E. Kieser, C. Rolfs, H. P. Trautvetter, and M. Wiescher, *Z. Phys. A* **305**, 319 (1982).
- ¹⁹P. B. Lyons, J. W. Toevs, and D. G. Sargood, *Nucl. Phys.* **A130**, 1 (1969).
- ²⁰C. Rolfs, A. M. Charlesworth, and R. E. Azuma, *Nucl. Phys.* **A192**, 257 (1973).
- ²¹T. Freye, H. Lorenz-Wirzba, B. Cleff, H. P. Trautvetter, and C. Rolfs, *Z. Phys. A* **281**, 211 (1977).
- ²²B. M. Paine and D. G. Sargood, *Nucl. Phys.* **A331**, 389 (1979).
- ²³O. Hausser, J. S. Lopes, H. J. Rose, and R. D. Gill, Nuclear Physics Conference Report, Oxford, 1966 (unpublished).
- ²⁴F. Ajzenberg-Selove and C. L. Busch, *Nucl. Phys.* **A336**, 1 (1980).
- ²⁵C. Rolfs, *Nucl. Phys.* **A217**, 29 (1973).
- ²⁶L. J. B. Goldfarb, in *Nuclear Reactions*, edited by P. M. Endt and M. Demeur (North-Holland, Amsterdam, 1959), Vol. 1, p. 159.
- ²⁷D. E. Alburger, D. J. Millener, and D. H. Wilkinson, *Phys. Rev. C* **23**, 473 (1981).
- ²⁸W. Bohne, C. K. Gelbke, P. Braun-Munzinger, W. Grauchulski, H. L. Harney, and H. Oeschler, *Nucl. Phys.* **A222**, 117 (1974).
- ²⁹J. R. Comfort, H. T. Fortune, J. V. Maher, and B. Zeidman, *Phys. Rev. C* **3**, 1086 (1971).
- ³⁰H. T. Fortune, H. G. Bingham, J. D. Garret, and R. Middleton, *Phys. Rev. C* **7**, 136 (1973).
- ³¹J. Szabo, J. Csikai, and M. Varnagy, *Nucl. Phys.* **A195**, 527 (1972).
- ³²M. Wiescher *et al.* (unpublished).
- ³³N. A. Roughton, M. J. Fritts, R. J. Peterson, C. A. Zaidins, and C. J. Hansen, *Astrophys. J.* **204**, 302 (1976); *At. Data Nucl. Data Tables* **23**, 177 (1979).
- ³⁴W. E. Burcham and J. M. Freeman, *Philos. Mag.* **40**, 807 (1949); **41**, 337 (1950).
- ³⁵G. G. Buch and D. J. Livesey, *Philos. Mag.* **46**, 824 (1955).
- ³⁶L. G. Earwaker and J. H. Montague, *Nucl. Phys.* **A109**, 507 (1968).